Figure S1

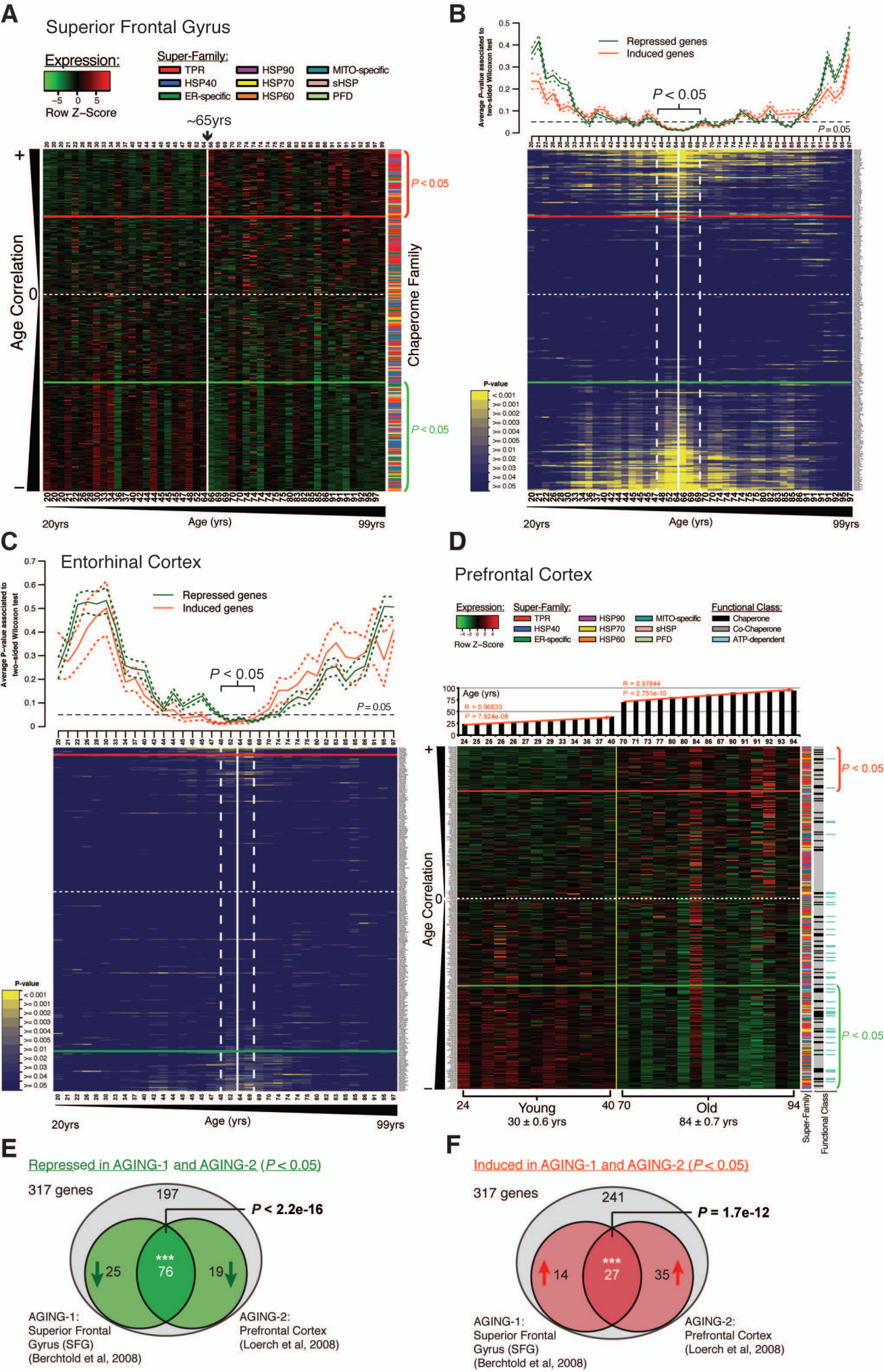
A
Superior Frontal Gyrus
Expression:
−5 0 5
Row Z–Score
Super-Family:
TPR
HSP40
ER-specific
HSP90
HSP70
HSP60
MITO-specific
sHSP
PFD
~65yrs
P < 0.05
Chaperome Family
P < 0.05
Age Correlation
+
0
–
20yrs
Age (yrs)
99yrs
B
Average P-value associated to two-sided Wilcoxon test
Repressed genes
Induced genes
P < 0.05
P = 0.05
P-value
< 0.001
>= 0.001
>= 0.002
>= 0.003
>= 0.004
>= 0.005
>= 0.01
>= 0.02
>= 0.03
>= 0.04
>= 0.05
20yrs
Age (yrs)
99yrs
C
Entorhinal Cortex
Average P-value associated to two-sided Wilcoxon test
Repressed genes
Induced genes
P < 0.05
P = 0.05
P-value
< 0.001
>= 0.001
>= 0.002
>= 0.003
>= 0.004
>= 0.005
>= 0.01
>= 0.02
>= 0.03
>= 0.04
>= 0.05
20yrs
Age (yrs)
99yrs
D
Prefrontal Cortex
Expression:
Row Z–Score
Super-Family:
TPR
HSP40
ER-specific
HSP90
HSP70
HSP60
MITO-specific
sHSP
PFD
Functional Class:
Chaperone
Co-Chaperone
ATP-dependent
Age (yrs)
R = 0.96633
P = 7.924e-08
R = 0.97844
P = 2.751e-10
P < 0.05
Age Correlation
+
0
–
P < 0.05
24
Young
30 ± 0.6 yrs
40 70
Old
84 ± 0.7 yrs
94
Super-Family
Functional Class
E
Repressed in AGING-1 and AGING-2 (P < 0.05)
317 genes
197
P < 2.2e-16
25
***
76
19
AGING-1:
Superior Frontal
Gyrus (SFG)
(Berchtold et al, 2008)
AGING-2:
Prefrontal Cortex
(Loerch et al, 2008)
F
Induced in AGING-1 and AGING-2 (P < 0.05)
317 genes
241
P = 1.7e-12
14
***
27
35
AGING-1:
Superior Frontal
Gyrus (SFG)
(Berchtold et al, 2008)
AGING-2:
Prefrontal Cortex
(Loerch et al, 2008)

Figure S2

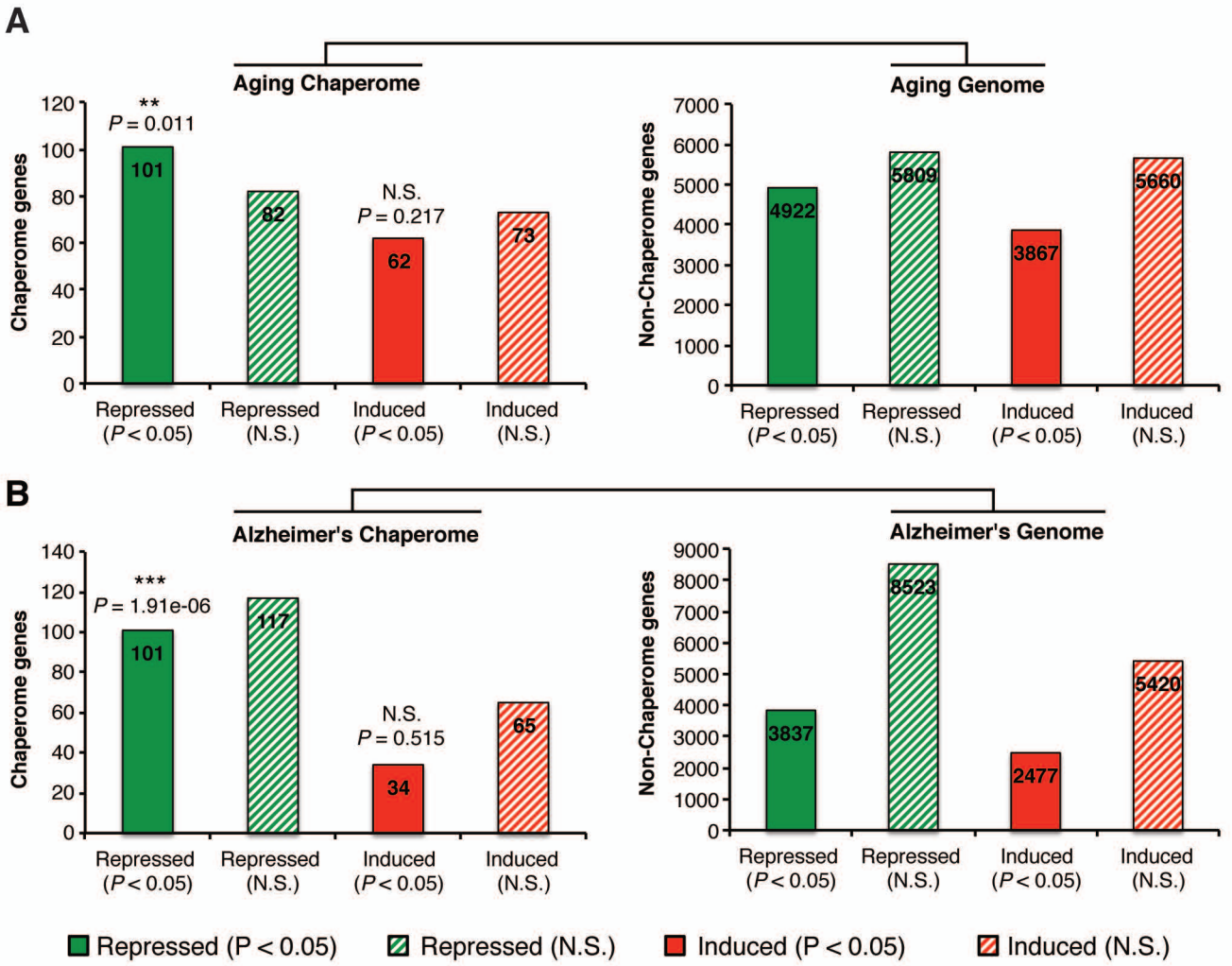
A
Aging Chaperome
Aging Genome
Chaperome genes
Non-Chaperome genes
** P = 0.011
N.S. P = 0.217
101
82
62
73
4922
5809
3867
5660
Repressed (P < 0.05)
Repressed (N.S.)
Induced (P < 0.05)
Induced (N.S.)
B
Alzheimer's Chaperome
Alzheimer's Genome
*** P = 1.91e-06
N.S. P = 0.515
101
117
34
65
3837
8523
2477
5420
Repressed (P < 0.05)
Repressed (N.S.)
Induced (P < 0.05)
Induced (N.S.)

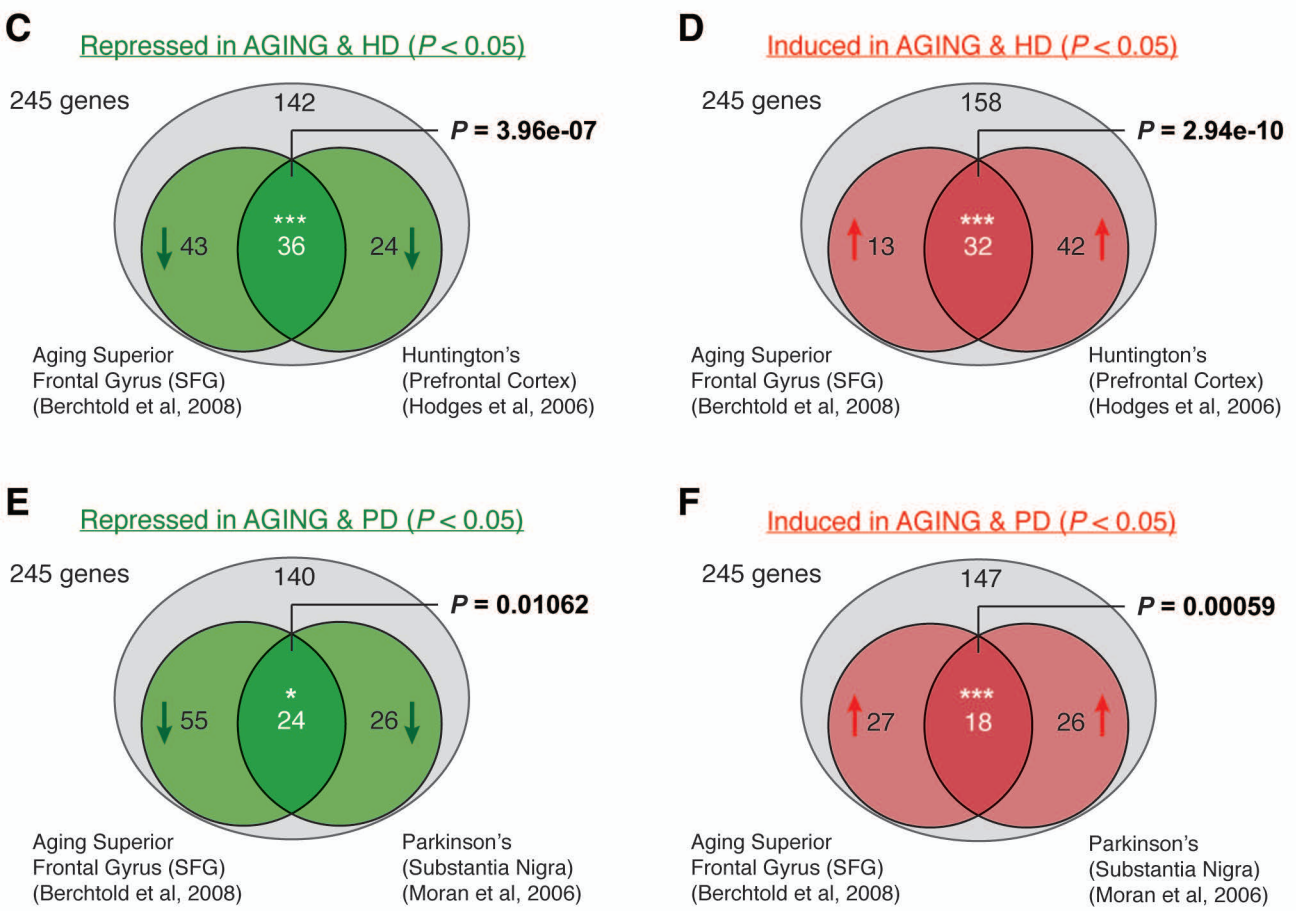
C
Repressed in AGING & HD (P < 0.05)
245 genes
142
P = 3.96e-07
43
***
36
24
Aging Superior Frontal Gyrus (SFG) (Berchtold et al, 2008)
Huntington's (Prefrontal Cortex) (Hodges et al, 2006)
D
Induced in AGING & HD (P < 0.05)
245 genes
158
P = 2.94e-10
13
***
32
42
Aging Superior Frontal Gyrus (SFG) (Berchtold et al, 2008)
Huntington's (Prefrontal Cortex) (Hodges et al, 2006)
E
Repressed in AGING & PD (P < 0.05)
245 genes
140
P = 0.01062
55
*
24
26
Aging Superior Frontal Gyrus (SFG) (Berchtold et al, 2008)
Parkinson's (Substantia Nigra) (Moran et al, 2006)
F
Induced in AGING & PD (P < 0.05)
245 genes
147
P = 0.00059
27
***
18
26
Aging Superior Frontal Gyrus (SFG) (Berchtold et al, 2008)
Parkinson's (Substantia Nigra) (Moran et al, 2006)

Figure S3

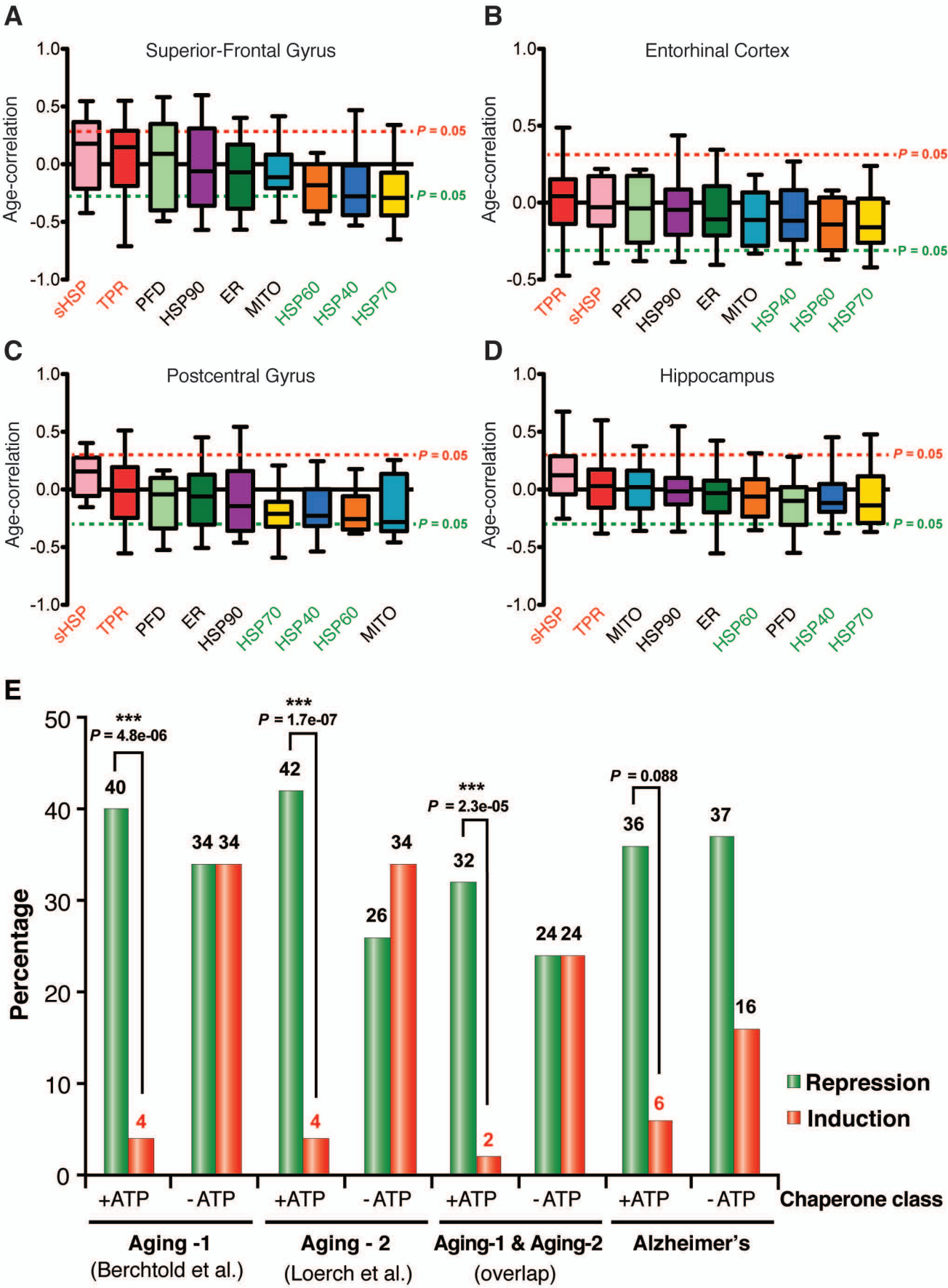
A
Superior-Frontal Gyrus
Age-correlation
1.0
0.5
0.0
-0.5
-1.0
P = 0.05
P = 0.05
sHSP
TPR
PFD
HSP90
ER
MITO
HSP60
HSP40
HSP70
B
Entorhinal Cortex
Age-correlation
P = 0.05
P = 0.05
TPR
sHSP
PFD
HSP90
ER
MITO
HSP40
HSP60
HSP70
C
Postcentral Gyrus
Age-correlation
P = 0.05
P = 0.05
sHSP
TPR
PFD
ER
HSP90
HSP70
HSP40
HSP60
MITO
D
Hippocampus
Age-correlation
P = 0.05
P = 0.05
sHSP
TPR
MITO
HSP90
ER
HSP60
PFD
HSP40
HSP70
E
Percentage
50
40
30
20
10
0
***
P = 4.8e-06
40
4
34 34
***
P = 1.7e-07
42
4
26
34
***
P = 2.3e-05
32
2
24 24
P = 0.088
36
6
37
16
Repression
Induction
+ATP
- ATP
+ATP
- ATP
+ATP
- ATP
+ATP
- ATP
Chaperone class
Aging -1
(Berchtold et al.)
Aging - 2
(Loerch et al.)
Aging-1 & Aging-2
(overlap)
Alzheimer's

Figure S4

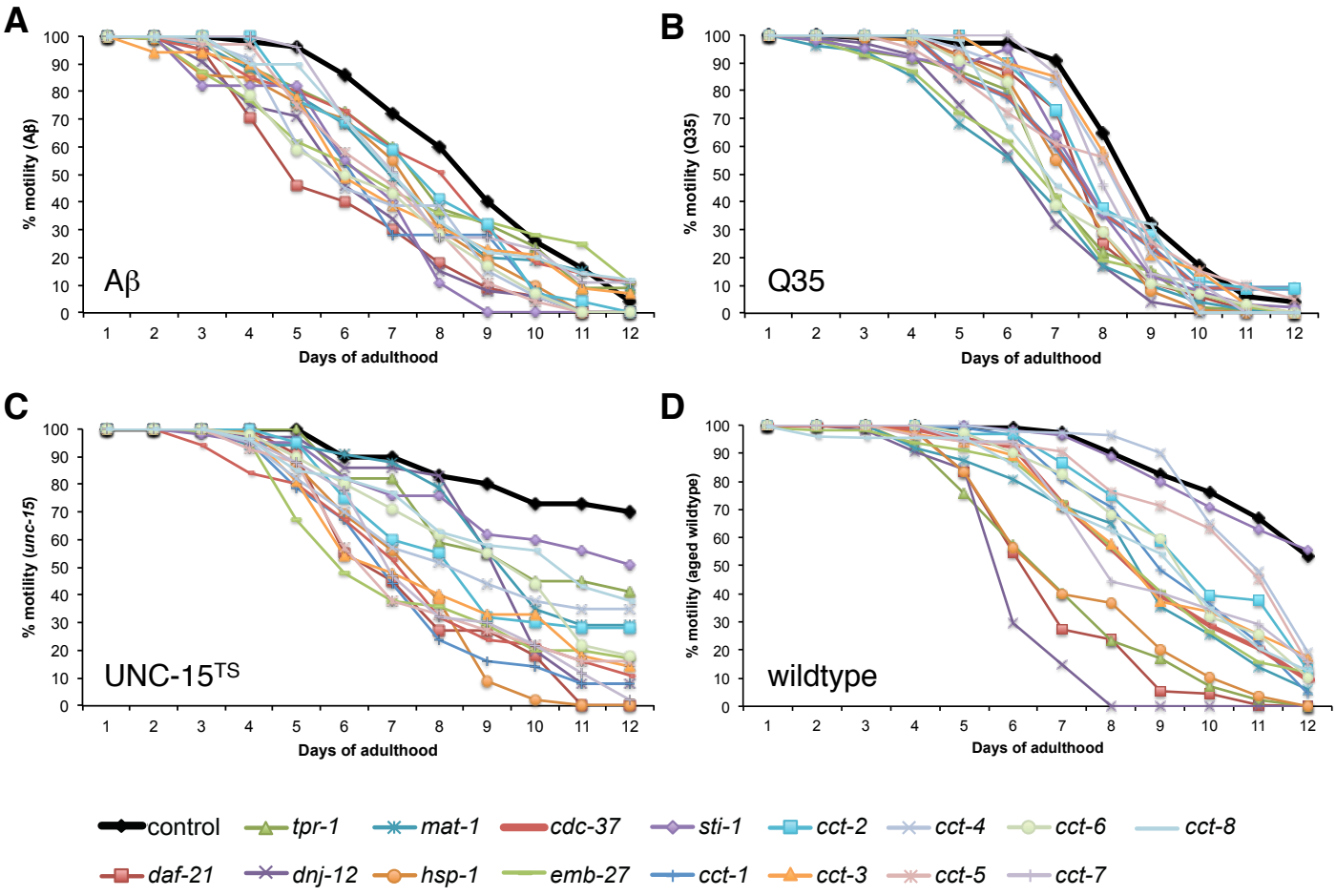
A
% motility (Aβ)
Aβ
Days of adulthood
B
% motility (Q35)
Q35
Days of adulthood
C
% motility (unc-15)
UNC-15TS
Days of adulthood
D
% motility (aged wildtype)
wildtype
Days of adulthood
control
tpr-1
mat-1
cdc-37
sti-1
cct-2
cct-4
cct-6
cct-8
daf-21
dnj-12
hsp-1
emb-27
cct-1
cct-3
cct-5
cct-7

Figure S5

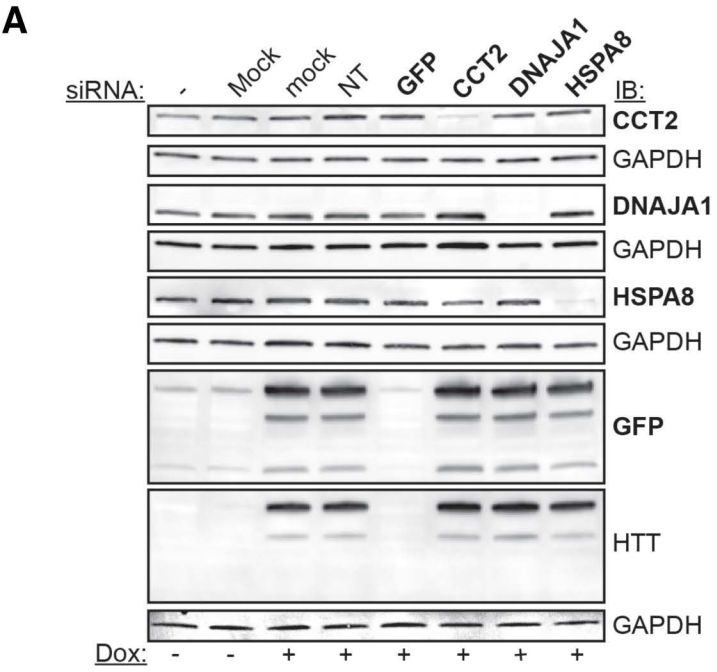

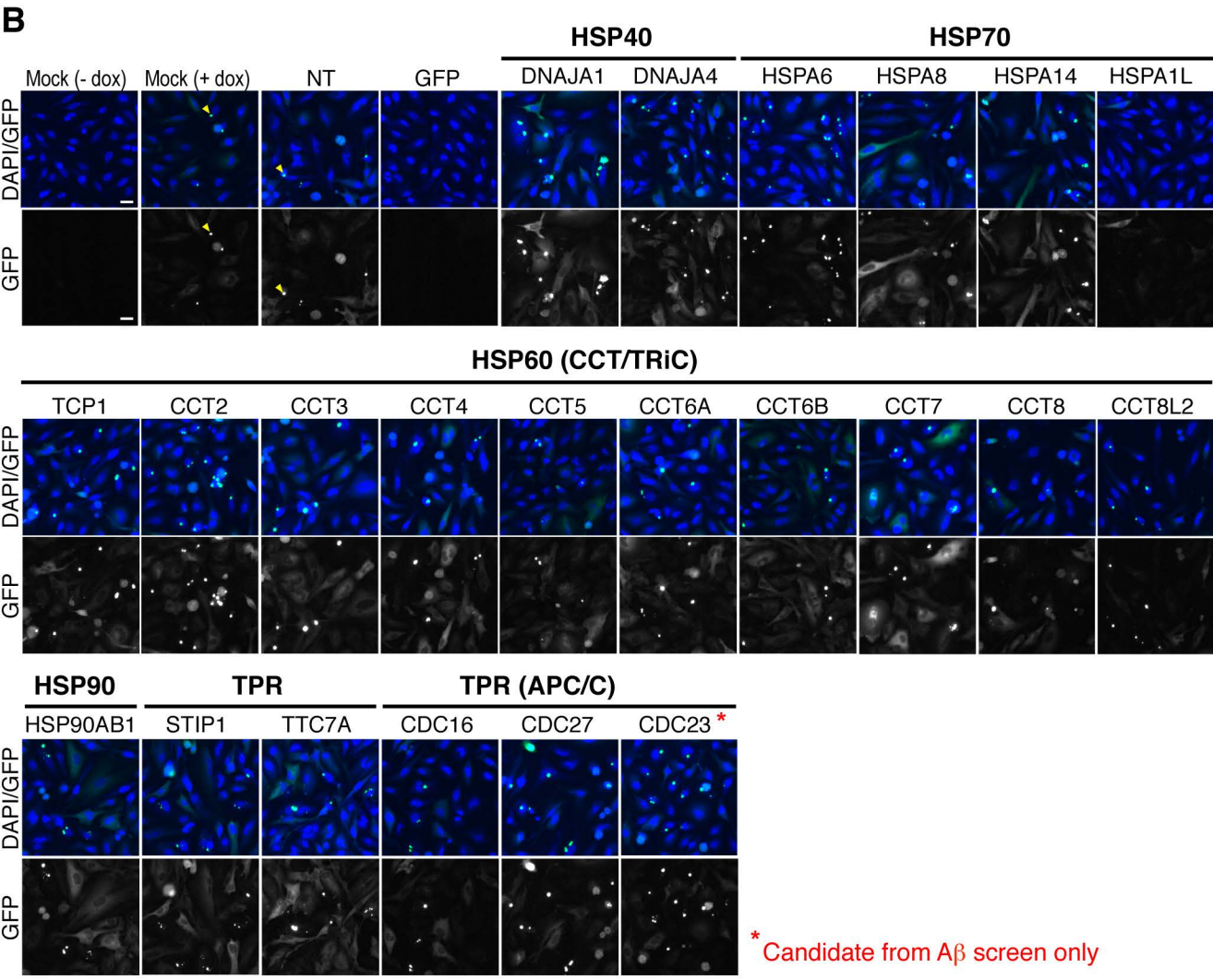

*Candidate from Aβ screen only

Figure S6

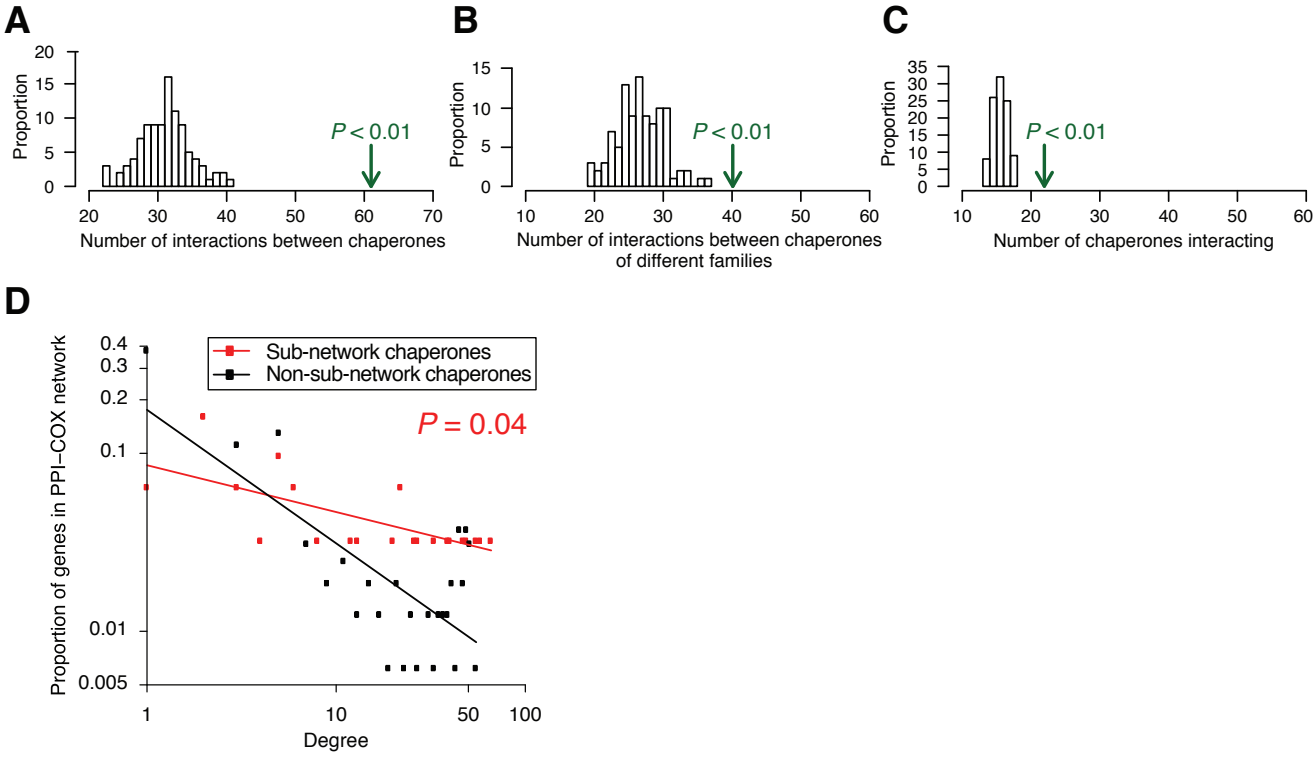
A
Proportion
P < 0.01
Number of interactions between chaperones
B
Proportion
P < 0.01
Number of interactions between chaperones of different families
C
Proportion
P < 0.01
Number of chaperones interacting
D
Sub-network chaperones
Non-sub-network chaperones
P = 0.04
Proportion of genes in PPI–COX network
Degree

Supplemental Figure Legends

Figure S1. Significant Clusters of Isochronic Differential Chaperome Induction and Repression in Human Aging Brains with Confirmation in an Independent Dataset, Related to Figure 1

A. Heat map showing 318 chaperones expressed in human brain (super frontal gyrus) ordered by decreasing correlation coefficients between age and gene expression (rows). Samples are ordered by chronologically increasing age with no clustering. The white dashed line indicates the gene with an age-expression correlation coefficient closest to zero. Chaperome genes above the red line are significantly induced by aging ($P < 0.05$), while the chaperone genes below the green line are significantly repressed by aging ($P < 0.05$). The y-axis color code visualizes the nine chaperome super-families. **B.** Two-sided Wilcoxon tests were performed on the chaperome aging heat maps to identify the age when the chaperome exhibits the most significant changes on the transcriptional level (Superior Frontal Gyrus). Genes are ordered by decreasing correlation of gene expression with age and samples are arranged by increasing age in chronological order to identify the age-span reflecting the most significant changes on the transcriptional level. Significant induction or repression of chaperones is observed between the early 50s to late 60s ($P < 0.05$) and peaks at ~65 years of age, which is also the mean age of onset of Alzheimer's Disease (Brookmeyer et al. 1998). **C.** Two-sided Wilcoxon tests performed as in B. on chaperome aging gene expression heat maps in Entorhinal Cortex. **D.** Heat map showing 318 chaperones expressed in human brain (Prefrontal Cortex) ordered by decreasing correlation coefficients between age and gene expression (rows). Samples are ordered chronologically by increasing age with no clustering (also see Figure S1). The white dashed line indicates the gene with an age-expression correlation coefficient closest to zero. Chaperome genes above the red line are significantly

induced by aging ($P < 0.05$), while the chaperone genes below the green line are significantly repressed by aging ($P < 0.05$). The y-axis color code visualizes from left to right the nine chaperome super-families, chaperone (black) and co-chaperone (grey) functional classes and ATP-dependent chaperones (turquoise) (compare Figure 1). **E-F.** Venn diagrams of genes significantly **E)** repressed ($P < 2.2e-16$) and **F**) induced ($P = 1.7e-12$) in comparable tissues from two independent datasets of human brain aging overlap significantly. Datasets used: AGING-1: Super Frontal Gyrus, aging dataset GSE11882 (Berchtold et al. 2008); AGING-2: Prefrontal Cortex, aging dataset (PMID:18830410) (Loerch et al. 2008).

Figure S2. Significance of Broad Chaperome Repression in Human Brain Aging and Alzheimer's Disease Compared to the Global Trend in the Genome and Significant Overlap of Chaperome Repression and Induction between Aging and Disease, Related to Figures 1 and 2

A. Broad repression of 32% (101 genes) of chaperome genes expressed in human aging brain (Superior Frontal Gyrus, (Berchtold et al. 2008)) is significant ($P = 0.01098$) compared to the global repression trend in the genome (20,258 genes, of which 4,922 non-chaperome genes are significantly repressed), while chaperome induction is not significant. **B.** Concordantly, broad repression of 32% (101 genes) of chaperome genes expressed in brains (Superior Frontal Gyrus, (Liang et al. 2008)) of Alzheimer's disease patients compared to age-matched controls is also significant (*** $P = 1.908e-06$) compared to the global trend in the genome (20,257 genes, of which 3,837 non-chaperome genes are significantly repressed), while induction of chaperome genes is not significant. **C-E.** Venn Diagrams showing overlaps between significantly induced and repressed human chaperome genes. Datasets used: AGING-1: Super Frontal Gyrus (SFG), dataset GSE11882 by Berchtold et al, PNAS 2008;

HD: Prefrontal Cortex (PFC), dataset GSE3790 (Hodges et al. 2006); PD: Substantia Nigra (SN), dataset GSE20295 (Moran et al. 2006). Chaperones and co-chaperones significantly induced and repressed ($P < 0.05$) in aging human brains and brains from AD patients compared to controls were identified amongst 317 chaperones and co-chaperones expressed in human brain and detected in both corresponding datasets. **C-D.** Overlap between genes significantly repressed or induced in SFG of human aging brain and in PFC of HD patients are significant. **E-F.** Overlaps between genes significantly repressed or induced in SFG of human aging brain and in SN of PD patients are significant.

Figure S3. Reproducible Functional Family Distribution of Chaperome Gene Expression Dynamics in Four Different Tissues from Human Aging Brains and Preferential Repression of ATP-dependent over ATP-independent Chaperones, Related to Figures 1 and 2

A-D. Boxes and Whiskers plots showing range of aging-correlation of each chaperome functional family and overall family distribution of aging-correlation arranged by decreasing median age-correlation for each super-family. Whiskers indicate minimum and maximum age-correlation observed amongst members of each super-family. Boxes outline the 25^{th} and 75^{th} percentile. Bars indicate the median age-correlation amongst all members of the super-family. Age-correlation observed for repressed and induced genes at *P*-value cut-off $P = 0.05$ in each dataset is indicated. Tissues are: **A:** Superior Frontal Gyrus, **B:** Entorhinal Cortex**, C:** Postcentral Gyrus**,** and **D:** Hippocampus. Dataset GSE11882, (Berchtold et al. 2008). **E.** Comparison of % fractions of ATP-dependent (total = 50) and ATP-independent (total = 38) chaperones present in the respective sets of significantly induced or significantly repressed genes in 1) Aging Super Frontal Gyrus (SFG), Aging-1 dataset GSE11882, (Berchtold et al.

2008); 2) Aging Prefrontal Cortex, Aging-2 dataset (PMID:18830410), (Loerch et al. 2008); 3) Superior Frontal Gyrus of Alzheimer's Disease patients versus controls (AD) gene expression dataset (GSE5281),(Liang et al. 2008).

Figure S4. Chaperome Subset RNAi significantly enhances paralysis phenotypes, Related to Figures 3 and 4

Individual data points shown for chaperome subset RNAi functional data shown in Figure 3 G and H and Figure 4 A and B. **A.** RNAi paralysis phenotype (% motility) observed in $A\beta_{42}$ expressing *C. elegans* throughout adulthood (days 1 to 12). Data points are means (n ≥ 3 independent experiments and n ≥ 25 animals / trial). **B.** RNAi paralysis phenotype (% motility) observed in Q35 expressing *C. elegans* throughout adulthood. Data points are means (n ≥ 3 independent experiments and n ≥ 25 animals / trial). **C.** RNAi paralysis phenotype (% motility) observed in *unc-15(e1402)* TS-strain at 15ºC throughout adulthood. Data points are means (n ≥ 3 independent experiments and n ≥ 20 animals / trial). **D.** RNAi paralysis phenotype (% motility) observed in aged wild-type-animals throughout adulthood. Data points are means (n ≥ 3 independent experiments and n ≥ 20 animals / trial).

Figure S5. The Human Chaperome Subset Safeguards Proteostasis to Prevent Huntingtin Aggregation, Related to Figure 5

A. Validation of siRNA knockdown efficiency of HTT-GFP, CCT2, DNAJA1 and HSPA8 by immunoblotting. **B.** Representative cellular images for siRNA knock-down of GFP (positive control) and chaperome sub-netowork targets representative of the five functional chaperome families present in the chaperome subset (HSP40s, HSP60s, HSP70s, HSP90s, TPR (APC/C)) are shown. NT = non-targeting siRNA. The yellow arrows highlight Htt-GFP aggregates. Scale bar, 20μm.

Figure S6. Significance of Human Chaperome Sub-Network Network Inter-Connectivity, Related to Figure 6

A-C. Significant inter-connectivity of the human orthologous chaperome sub-network interactome compared to 100 randomized PPI-COX chaperome networks. PPI-COX network randomizations were performed keeping the number of nodes, edges and node degree constant while rewiring edges between nodes. PPI and COX edges were treated separately. **A.** Number of interactions between chaperones, **B.** number of interactions between chaperones of different families, and **C.** the number of chaperones interacting were significant ($P < 0.01$) compared to the numbers observed in 100 randomized PPI-COX networks. **D.** Proportion of genes in the PPI-COX network and their degree distribution. Sub-network chaperones have a significantly higher degree than the rest of the PPI-COX chaperome network nodes, i.e. non-sub-network chaperones ($P = 0.04$, Wilcoxon test).

Supplemental Table Legends

Table S1. Chaperome Super-Family InterPro Criteria Domains, Related to Figure 1

44 unique IPR-IDs representing *bona-fide* InterPro domains used as criteria domains for chaperome gene list curation and annotation into 9 functional super-families. IPR-IDs, corresponding *bona-fide* functional chaperone and co-chaperone families, respective parent super-families as well as super-family color-codes are indicated.

Table S2. The Chaperome Database, Related to Figures 1 and 3

Tab S2A. 332 human chaperones and co-chaperones constituting the human chaperome. Uniprot identifier, HGNC gene symbol, InterPro domains and match to our chaperome

ontology categorization, chaperome family ontology, compartment, gene name, gene description as well as worm orthologs are indicated. Related to Figure 1. **Tab S2B.** 219 worm chaperones and co-chaperones constituting the worm chaperome. ENSEMBL identifier, WBase gene ID and gene symbol, InterPro domains and match to our chaperome ontology categorization, chaperome family ontology, compartment, gene name, gene description as well as human orthologs are indicated. Related to Figure 3.

Table S3. Human Chaperome Gene Expression Correlation in Brain Aging and Disease, Related to Figures 1 and 2

Tab S3A. 318 human chaperome genes ordered by their correlation of gene expression with age in Superior Frontal Gyrus, Postcentral Gyrus, Entorhinal Cortex and Hippocampus of human brains (Berchtold et al. 2008) in decreasing order. * $P < 0.05$, ** $P < 0.01$, *** $P < 0.001$, Student's t test. **Tab S3B.** 318 human chaperome genes ordered by their correlation of gene expression with age in Prefrontal Cortex of human brain (Loerch et al. 2008) in decreasing order. * $P < 0.05$, ** $P < 0.01$, *** $P < 0.001$, Student's t test. **Tab S3C.** 318 human chaperome genes ordered by their correlation with gene expression in human brain Superior Frontal Gyrus (Berchtold et. al, PNAS 2008) in decreasing order. Correlation of gene expression in the three neurodegenerative diseases AD ((Liang et al. 2008)), HD (Hodges et al. 2006) and PD (Moran et al. 2006) is indicated as ratio over normal (control patients). **Tab S3D.** Overlaps of human chaperome genes significantly repressed in Aging (Superior Frontal Gyrus, (Berchtold et al. 2008)) and significantly repressed in AD (Superior Frontal Gyrus), HD (Prefrontal Cortex) and/or PD (substantia nigra). AD, HD, and PD disease gene expression datasets are from: AD (Liang et al. 2008), HD (Hodges et al. 2006) and PD

(Moran et al. 2006). **Tab S3E.** Overlaps of human chaperome genes significantly induced in Aging and significantly induced in AD, HD and/or PD. Tissues and datasets as in S5A.

Table S4. Human Chaperome Physical Protein-Protein Interactions, Related to Figures 2 and 6

Tab S4A. 206 unique protein-protein interactions between human brain-expressed chaperones from public databases. Source database name, cited publication (PubMed ID) and interaction discovery method are indicated, respectively. **Tab S4B.** 40 homodimers were excluded from the network analysis.

Table S5. Human Chaperome Brain Aging Co-Expression Correlation, Related to Figures 2 and 6

50,403 all-by-all pairs representing 318 human chaperome genes expressed in human brain (Superior Frontal Gyrus, (Berchtold et al. 2008)). Pearson co-expression correlation coefficients for each pair were calculated based on gene expression in human brain. COX edges with a Pearson co-expression correlation coefficient with aging (corr > 0.8) were designated as COX. 1,193 COX edges represent significantly co-expressed chaperones in human brains.

Table S6. Human Chaperome Physical and Brain Co-Expression (PPI-COX) Chaperome Network and Aging-Response Communities, Related to Figures 2 and 6

Tab S6A. In this network, there are 5,004 pairs of interactions, of which 714 are PPIs, 4,226 are COX (corr > 0.8), and 64 are both PPI and COX. There are 66 pairs in induction communities and 4,098 pairs in repression communities. **Tab S6B.** The unique pairs are in

parentheses and listed separately in **S6B**. There is a total of 40 communities, of which 6 are induction communities and 34 are repression communities.

Table S7. Human Chaperome Sub-Network Functional Validation, Related to Figures 3, 4, and 5

16 C. elegans chaperone and co-chaperone hits from Ab and polyQ RNAi screens constituting the "chaperome subset". Paralysis phenotypes are indicated as % motility. 28 human orthologs are color-coded according to their siRNA phenotype in a HeLa cellular model of Huntingtin-exon1(Q78)-GFP cytoplasmic clearance and aggregation.

Supplemental Experimental Procedures

Chaperome Gene List Curation, Annotation and Orthology Mapping

We curated the literature for chaperone and co-chaperone families covering all structural and functional categories and the major subcellular localizations relevant to chaperone-assisted protein folding and annotated family members known at present for human and *C. elegans* in detail including for human the respective Entrez gene IDs, Uniprot identifiers, gene symbols, cellular compartment, Uniprot description and Entrez gene description (Chang et al. 2007; Tang et al. 2007; Heldens et al. 2010; Braakman and Bulleid 2011). We then matched domain structures as referenced by the UniProt database to each gene and prioritized *bona-fide* InterPro protein domain identifiers (IPR-IDs) characteristic of each family to i) consolidate our literature-based annotation and ii) to search for additional structurally similar family members not previously associated with the respective families in the literature. We determined 9 top-level functional chaperome super-families based on curated literature evidence as well as based on a curated selection of *bona-fide* IPR-domains (referenced by IPR-IDs) (Table S1)

found in these established functional families. Chaperones and co-chaperones curated in the literature as members of one of these nine super-families or genes containing at least one of these IPR-domains were consequently grouped accordingly into the nine functional super-families, including the HSP60, HSP70, HSP90 and Prefoldin (PFD) folding machines, small HSPs (sHSPs). The specific complement of chaperones that have evolved to function exclusively within the ER and mitochondrial (MITO) subcellular compartment were grouped as 'ER-specific' and 'MITO-specific'. Smaller co-chaperone families such as the cyclophilins, FKBPs with clear functional association with a chaperone host were concordantly co-grouped within the respective chaperone system, such as the HSP90 system or the HSP70 system in the case of Bag proteins or the GrpE nucleotide exchange factors (NEFs). More promiscuous co-chaperones such as the HSP40 and TPR-domain containing co-chaperones, however were grouped as separate super-families. Consequently chaperome super-family grouping was systematic such that we first considered a guilt-by-association principle for specific pre-curated sets of *bona-fide* IPR criteria domains. Consequently, chaperones were grouped by their functionality first, regardless of their subcellular localization. MITO-specific and ER-specific super-family members represent those chaperones and co-chaperones, for which no IPR-domain match strings were obtained. These were curated and grouped based on on literature knowledge and functional evidence of compartment-specific localization and/or function.

To complement human and worm chaperome gene set annotations with phylogenetic relationships between the two species we identified human and worm orthologues by automated orthology mapping using the NCBI HomoloGene database. In a second step we re-curated the annotations based on the WormBase database (release WS234) comparative genomics tool, which associates each worm gene entry with human orthologous based on

curated and automated predictions by NCBI KOGS, InParanoid, TreeFam, precomputed BLAST results, Ensembl COMPARA and the orthologs matrix project (OMA) (Harris et al. 2010; 2012; Sayers et al. 2012). We applied bipartite mapping according to our annotation criteria to compare worm and human chaperomes and identified the overlapping as well as the respective species-specific chaperome subsets.

Chaperome Expression Correlation Analyses

We extracted expression profiles for 318 human chaperome genes from human Superior Frontal Gyrus, Entorhinal Cortex, postcentral gyrus and Hippocampus brain biopsy tissue samples of aged subjects (dataset accessible under GEO accession number GSE11882) (Berchtold et al. 2008) and from an additional independent dataset derived from human Prefrontal Cortex (Loerch et al. 2008). Original expression data are fitted by linear model using R package Limma at log2 scale, with age and gender as variables. After model fitting, we subtracted the portion of gene expression associated with gender cofactor so that the processed data are only associated with age cofactor. Among multiple probe sets of a gene, we kept the probe set whose expression was most significantly changed with age, according to the adjusted *P*-value associated with the coefficient of age cofactor in the linear model. Chaperome age expression correlation coefficients (corr) and *P*-values were calculated using cor.test function in the R stats package and applying default arguments. Chaperome genes with significantly induced or repressed expression during human brain aging were identified at a *P*-value cutoff of < 0.05. We used distance measures defined by 1-[Pearson_correlation_coefficient] to create a distance matrix comparing chaperome pairs, where correlation coefficients were calculated using the cor function in the R stats package applying default arguments. Hierarchical clustering was performed on the calculated distance matrix using hclust in the R stats package with default arguments and displayed as a heat

map with dendrogram using heatmap.2 in the R gplots package and dendrogram display. To estimate chaperome induction and repression cluster boundaries we ordered aging samples chronologically from 20 to 99 years old. We computed Wilcoxon signed-rank tests (Bauer 1972) for each chaperome gene at each age to evaluate the difference between the expression values of the gene below and above that specific age (the corresponding age cutoff being categorized in the higher age category) and the significances were estimated by the *P*-value of the Wilcoxon test. We averaged *P*-value obtained for all genes at each age cutoff to determine overall most significant age. Brain biopsy samples from AD, PD and HD patients were analyzed as described above. Correlation of expression was determined as ratio of average expression in disease over controls.

Chaperome Network Community Clustering

Genes significantly induced or repressed in aging with $P < 0.05$ were defined as significantly aging-correlated. We analyzed the PPI-COX network to identify clusters of edges that connect subsets of nodes using the link-community algorithm (Ahn et al. 2010), which allows clustering of graph edges such that nodes can be part of different communities. We considered communities with ≥ 2 edges and thus ≥ 3 nodes, and containing only induced or only repressed nodes. Link communities are based on significance of aging-correlation and network connectivity taking both PPI and COX edges into account. Controlled by network randomization trials this approach allowed us to re-prioritize 15 genes not significantly aging-correlated ($P \geq 0.05$) based on their membership in link communities and to de-prioritize 35 genes with significant aging-correlation based on their absence from communities.

In order to evaluate connectivity of the chaperome network, we built 100 randomized PPI-COX networks, keeping the number of nodes, edges and node degrees constant while

rewiring edges between nodes. PPI and COX edges were treated separately to conform to the different nature of the interaction.

C. elegans RNAi Screens for Chaperome Modifiers of Protein Misfolding, Aging-related Proteotoxicity and Myofilament Structure

We performed chaperome-wide RNAi screens for enhancement of motility defects in *C. elegans* muscle cells with the commercial RNAi library and additional candidates cloned into L4440, transformed into *E. coli* strain HT115(DE3) (Kamath and Ahringer 2003). RNAi bacterial cultures were grown for 12 hours in LB-ampicillin 50 ug/ml, at 37°C and induced with 1mM isopropyl B-D-thiogalatoside (IPTG, Sigma) for 4 hours at 37°C. Cultures were plated on agar containing IPTG (1.429 g/L), ampicillin (.075 g/L), and tetracycline (.0125 g/L). To obtain an age-synchronized population, eggs were harvested from gravid hermaphrodites, hatched overnight at 20°C and arrested at the first larval stage (L1). The next day, 35-40 arrested L1 worms were plated on agar with chaperome RNAi bacteria and incubated at 20°C. Adult worms were transferred to new RNAi plates daily to separate adults from progeny, and scored for paralysis ($A\beta_{42}$ screen) on day 4 or for motility defects (Q35 screen) on day 2 of adulthood.

Aβ expressing worms that did not move when prodded with a needle were scored as paralyzed (Link 1995). Q35 expressing worms' movements were digitally recorded using a Leica M205 FA microscope with a Hamamatsu digital camera C10600-10B and the Hamamatsu SimplePCI imaging software. Animal positions were determined using ImageJ. Animals were tracked throughout a 30-second movie and track-length was calculated as sum of lengths of all movement vectors. Average speed (pixels per frame) was the sum of all movement vectors divided by the total number of vectors (tracks). Speeds were converted from pixels per frame into μm/s (Silva et al. 2011). RNAi modifiers causing larval delays or

arrest were retested and fed to animals at L4 larval stage. RNAi modifiers, such as *unc-45*, that affected the motility of wildtype animals to the same extent during our screens were removed from further analysis. Animals fed chaperome candidates RNAi with a 20% decrease in movement compared to control animals were retested and RNAi candidates with a 20% decrease in movement compared to control in ≥ 3 experiments constitute the final set. For aging-related proteotoxicity, synchronized L1 animals expressing $A\beta_{42}$, polyQ or wild-type animals were fed bacteria expressing RNAi for each subset chaperone. When lethality or larval arrest were observed worms were fed at the L4 stage. Adult animals were assayed daily and those that did not respond to gentle prodding were scored as paralyzed. *unc-15(e1402)* animals were grown at 15°C and assayed daily for paralysis.

To examine the effect of chaperome subset gene down-regulation on myofilament folding and assembly in muscle cells (Herndon et al. 2002) (Sarcopenia readout), we monitored MYO-3::GFP fluorescence in animals fed with bacteria expressing dsRNA against each subset chaperone. Images were taken on day 1 and day 8 of adulthood using a Zeiss Axiovert 200 microscope.

siRNA Perturbation Coupled to High-Content Imaging (siRNA-HCI) Screen for Modifiers of Huntingtin (HTT) Cytoplasmic Clearance and Aggregation in HeLa Cells

Chaperome modifiers of Htt cytoplasmic clearance and aggregation were identified by siRNA perturbation coupled to high-content imaging (siRNA-HCI) in HeLa cells. Monoclonal doxycycline-inducible Tet-On HeLa cells expressing HTT(Q78)-exon1-GFP from a P_{CMV} promoter in the pLenti6.3/V5 vector were maintained in Dulbecco's Modified Eagle's Medium (DMEM) with 10% FBS, 1% penicillin/streptomycin (P/S), 2µg/ml Blasticidin and 200µg/ml G418. siRNA knock-downs were performed in 96-wells at initial cell density of 8,000 cells/well in 100µl DMEM and 10% FBS and 1% P/S. Twelve hours post seeding, cells were

mock - treated or treated with 10nM non-targeting, GFP or target-specific quadruplex Dharmacon smart-pool siRNAs in Optimem and 0.5µl Dharmafect #1. Twelve hours post transfection media were replaced and Htt(Q78)-exon1-GFP expression induced with 0.5µg/ml dox for 48 hours. After 72 hours of siRNA knock-down and 48 hours of induction, cells were fixed in para-formaldehyde and nuclei stained with Hoechst 33342 dye. Fixed cells were imaged using a Thermo Scientific Cellomics ArrayScan VTI HCS Reader. Cell number and % cells with one or more aggregates were quantified using co-localization and compartmental analysis algorithms. Knock-downs were carried out in triplicate and two biological repeats. Percentage of cells with ≥ one aggregate per cell were determined over doxycycline-induced mock-treated cells.

Immunoblot Validation of Chaperome Sub-Network siRNA Knockdown

Monoclonal doxycycline-inducible Tet-On HeLa cells expressing HTT(Q78)-exon1-GFP were maintained in DMEM medium under Blasticidin and G418 selection. siRNA knock-downs were performed as described above in 6-wells at initial cell density of 250,000 cells/well. After 72 hours of siRNA knockdown and 48 hours of induction, cells were washed in 1x PBS and lysed in 1x RIPA buffer with Roche Complete Mini protease inhibitor cocktail. Protein extracts were prepared in RIPA buffer and 10µg extract were separated by SDS-PAGE, probed with primary antibodies and consequently HRP-coupled secondary antibodies followed by chemoluminescent detection. Primary antibodies used were anti-CCT2, Cell Signaling #3561 rabbit polyclonal IgG at 1:1000 dilution; anti-DNAJA1 (HDJ2), Abcam ab126774 [EPR7248] rabbit monoclonal IgG at 1:1000 dilution; anti-HSPA8 (HSC70), Abcam ab1427 rabbit polyclonal IgG at 1:1000 dilution; anti-HTT, Millipore MAB5492 mouse monoclonal IgG_1 at 1:1000 dilution and anti-GFP, Roche 11814460001 (clones 7.1 and 13.1) at 1:1000 dilution followed by detection with HRP-coupled anti-mouse and anti-rabbit antibodies and

chemoluminescence detection. Each knock-down and western blot experiment was verified in two biological repeats.

Supplemental References

Ahn, Y. Y., J. P. Bagrow, et al. (2010). Link communities reveal multiscale complexity in networks. Nature 466(7307): 761-764.

Bauer, D. F. (1972). Constructing confidence sets using rank statistics. Journal of the American Statistical Association 67: 687-690.

Berchtold, N. C., D. H. Cribbs, et al. (2008). Gene expression changes in the course of normal brain aging are sexually dimorphic. Proceedings of the National Academy of Sciences of the United States of America 105(40): 15605-15610.

Braakman, I. and N. J. Bulleid (2011). Protein folding and modification in the mammalian endoplasmic reticulum. Annual review of biochemistry 80: 71-99.

Brookmeyer, R., S. Gray, et al. (1998). Projections of Alzheimer's disease in the United States and the public health impact of delaying disease onset. American journal of public health 88(9): 1337-1342.

Chang, H. C., Y. C. Tang, et al. (2007). SnapShot: molecular chaperones, Part I. Cell 128(1): 212.

Harris, T. (2012). WormBase release WS232.

Harris, T. W., I. Antoshechkin, et al. (2010). WormBase: a comprehensive resource for nematode research. Nucleic acids research 38(Database issue): D463-467.

Heldens, L., R. P. Dirks, et al. (2010). Co-chaperones are limiting in a depleted chaperone network. Cellular and molecular life sciences : CMLS 67(23): 4035-4048.

Herndon, L. A., P. J. Schmeissner, et al. (2002). Stochastic and genetic factors influence tissue-specific decline in ageing C. elegans. Nature 419(6909): 808-814.

Hodges, A., A. D. Strand, et al. (2006). Regional and cellular gene expression changes in human Huntington's disease brain. Human molecular genetics 15(6): 965-977.

Kamath, R. S. and J. Ahringer (2003). Genome-wide RNAi screening in Caenorhabditis elegans. Methods 30(4): 313-321.

Liang, W. S., E. M. Reiman, et al. (2008). Alzheimer's disease is associated with reduced expression of energy metabolism genes in posterior cingulate neurons. Proceedings of the National Academy of Sciences of the United States of America 105(11): 4441-4446.

Link, C. D. (1995). Expression of human beta-amyloid peptide in transgenic Caenorhabditis elegans. Proceedings of the National Academy of Sciences of the United States of America 92(20): 9368-9372.

Loerch, P. M., T. Lu, et al. (2008). Evolution of the aging brain transcriptome and synaptic regulation. PloS one 3(10): e3329.

Moran, L. B., D. C. Duke, et al. (2006). Whole genome expression profiling of the medial and lateral substantia nigra in Parkinson's disease. Neurogenetics 7(1): 1-11.

Sayers, E. W., T. Barrett, et al. (2012). Database resources of the National Center for Biotechnology Information. Nucleic acids research 40(Database issue): D13-25.

Silva, M. C., S. Fox, et al. (2011). A genetic screening strategy identifies novel regulators of the proteostasis network. PLoS genetics 7(12): e1002438.

Tang, Y. C., H. C. Chang, et al. (2007). SnapShot: molecular chaperones, Part II. Cell 128(2): 412.